

Experimental-Modeling Evaluation Between Hydraulic and Electrical Variables Using Copulas and Spectral Analysis for a Centrifugal Pump

V. O. Monsalve^{1,2}, F. Botero¹, L. F. Cardona^{2,3†} and V. J. Pugliese⁴

¹ *Applied Mechanics Research, Group, Mechanical Engineering Department, Universidad EAFIT, Medellín 050022, Colombia*

² *Pulp and Paper Research Group, Faculty of Chemical Engineering, Universidad Pontificia Bolivariana, Medellín 56006, Colombia*

³ *Department of Basic Sciences, Universidad Católica Luis Amigó, Medellín 050034, Colombia*

⁴ *Department of Mechanical Engineering, Universidad del Norte, Barranquilla 081001, Colombia*

†Corresponding Author Email: luis.cardonapa@amigo.edu.co

(Received October 2, 2022; accepted December 22, 2022)

ABSTRACT

Centrifugal pumps are turbomachines that have wide industrial applications and could perform in different ways such as pump and turbine mode. The maintenance of this equipment is mostly carried out using invasive methods that are expensive, time-consuming, and even complicated. The application of non-invasive methods is sought since they offer the advantage of real-time monitoring without stopping the process, reducing component assembly and disassembly times and providing a faster response. The aim of this work is done an experimental investigation that shows evidence about how the information on the hydraulic variables can be obtained if the electrical variables are monitored for the modes of operation such as pump and turbine. This work is divided into two parts, the first part is based on a statistical analysis to perform a multivariate adjustment through copulas and probability distributions. The second part focuses on the graphical analysis of the power density spectra for the hydraulic variables, the torque, and the defined electrical variables. The amplitude peaks of each variable and which peaks are common between them are determined. A statistically significant fit for Tawn type 2 copula is obtained with the indicator variable of pressure fluctuation and a multivariate transformation of the three-phase network currents. In the spectra analysis, common amplitude peaks are observed between the spectra that indicate the information flow on the phenomena between the hydraulic variables and the electrical variables.

Keywords: Copula analysis; Spectral analysis; Turbomachinery; Centrifugal pump; Turbine.

NOMENCLATURE

<i>AIC</i>	Akaike Information Criterion	<i>k</i>	number of deviations from the sample standard deviation
<i>C</i>	copula	<i>KS</i>	Kolmogorov-Smirnov
<i>CDF</i>	Cumulative Distribution Function	<i>LS</i>	upper limit
<i>D-T</i>	common peaks between Dytran and Torque	<i>Ln</i>	natural logarithm
<i>D-A</i>	common peaks between Dytran and Accelerometer	<i>R²</i>	determination coefficient
<i>D-A-T</i>	amplitude spikes that are common between Dytran, Accelerometer, and Torque variables	<i>W_{i;n}</i>	expectation of the statistic for K-plot variable distribution 1 or 2
<i>I</i>	amplitudes for the current 1, 2 and 3	<i>u_i</i>	distance of the observation to the center of the data for Chi plot
		<i>μ</i>	average
		<i>σ</i>	standard deviation

1. INTRODUCTION

Turbomachines are hydrodynamic equipment that uses a rotating impeller to transfer power from the motor to the fluid (Li *et al.* 2022) and are used in different applications such as chemical industry, manufacturing, agriculture, and transportation (Wang *et al.* 2022). A suitable design and operation of a centrifugal pump imply an efficient momentum, mass, and heat transfer to other process equipment such as heat exchangers, shock and mixing tanks, reactor systems, and distillation towers, among others (Perez 2022; Li *et al.* 2022; Wang *et al.* 2022).

The main turbomachines that can be found in industry are centrifugal pumps and turbines (Muttalli *et al.* 2014). A centrifugal pump in its structure does not differ significantly from a reaction hydraulic turbine. The difference lies mainly in its function since the pump transforms mechanical energy into hydraulic energy and the turbine does the reverse process. The design of each of them is then defined by the hydraulic efficiency for each application, efficiency that is determined by the constructive characteristics of the rotor, the spiral chamber, or the volute. It could then be stated that the efficiency in a hydraulic turbine application is greater at a specific condition (Flórez and Jiménez 2008).

In this energy transformation process, hydrodynamic phenomena can occur and affect the operation of the machine (Obidov *et al.* 2021). The consequences of these phenomena include loss of mass of the components, unbalanced rotation, and vibrations, among other results that decrease the efficiency of the pump (Al-Obaidi 2019; Perez 2022). The development of tools that allow the early detection of these phenomena has been the objective of different scientific and engineering works that seek to find the optimal operating conditions for hydrodynamic machines and maximize their life span. However, not only these tools are aimed to work, but also offer non-invasive methods that protect the integrity of the machines and reduce costs (Al-Obaidi 2019; Obidov *et al.* 2021; Li *et al.* 2022).

One of the most studied phenomena in turbomachines is cavitation (Li *et al.* 2022). Mousmoulis *et al.* (2019) carried out a review of the experimental studies for phenomenon detection and mentions four main methods to detect this irregularity and is related to static pressure, sound pressure, vibration acceleration, and fluid visualization. Al-Hashmi (2012) studied cavitation from acoustics in a centrifugal pump during normal operation. Al-Hashmi (2012) analyzed acoustic signal spectra, however, there is no clear relationship between pump cavitation and shaft frequency and its harmonics. Baldassarre (2018) did a study with a real-time image processing system for cavitation detection. Three different algorithms for real-time image analysis were developed and compared with a frequency diagram. In real-time, a response was obtained, which ensures the high reliability of cavitation detection.

The Rotating Stall phenomenon has also been studied with non-invasive methods. Ullum *et al.*

(2006) proposed two different methodologies for the detection of rotating stalls using velocity and pressure time series analysis. Also, velocity and pressure spectra analyses are done to determine if the rotating stall frequency could be identified. The results did not show significant sensitivity to flow rate, nor they were completely conclusive in detecting the frequency of rotating stalls in all the cases studied. Bolaños (2018) studied the phenomenon of Rotating Stall in a low specific speed centrifugal pump, the response of the turbomachine in the volute was analyzed in the time and frequency domain, through spectral components. Two types of phase analysis were performed using two different methods, cross-correlation, and Fourier phases. This last method was developed and proposed by the authors as an alternative to the cross-correlation method.

Non-invasive methods have been studied for both pump mode and turbine mode. Bolaños *et al.* (2019) used a centrifugal pump working as a turbine. Image processing of a sequence of photos taken with a high-speed camera was used, and pressure sensor signals were considered as pressure fluctuations. The analysis in the time and frequency domain allowed us to find the relationship between the torch spectra and the areas projected in the sequence of images of the phenomenon.

A practical way of identifying hydraulic phenomena is by evaluating the electrical variables of the system. The measurement of currents and voltages represents less effort and less cost compared to the measurement of variables such as pressure and flow. Machado *et al.* (2016) used a noninvasive technique to diagnose the hydrodynamic phenomenon of cavitation in real-time. The suction capacity was studied to analyze the electrical parameters and find the relationship between cavitation and the stator current spectrum. The proposal is based on the evaluation of the cavitation phenomenon using time-frequency transforms of the current stator. The results showed effectiveness at the moment of diagnosing the existence of cavitation.

A nonlinear multivariate adjustment methodology is applied through copulas, whose application is not so frequent in the study of turbomachines and has scarce exploration regarding the relationship between electrical variables and hydraulic variables. Taillon *et al.* (2019) developed a method of analysis of cavitation peaks (impact events) using copulas. Impact events, also known as spikes, are defined as maximums in the amplitude pressure applied to the surface of a material. The copulas allow the study of the dependency structure of the characteristics of the measured impacts. The measured parameters show that they are not independent but have a complex and asymmetric dependency structure. The copula is a better fit compared to a joint distribution of independent marginals (Taillon *et al.* 2019).

The present work aims to relate the hydraulic variables such as the pressure fluctuations and the vibrations of the turbomachine casing, the torque, and the electrical variables (non-invasive variables) of the three-phase network. The above implies three

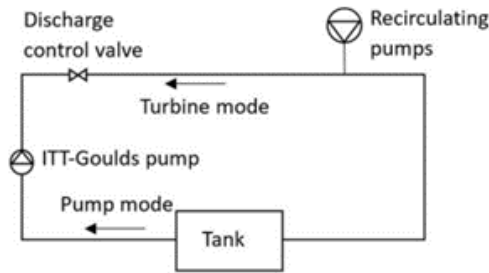


Fig. 1. General test bench scheme (Bolaños and Botero 2021).

currents and the three voltage drops of each line. Two methodologies are applied for the pump and turbine operation modes, firstly a statistical analysis using copulas is done, where pressure fluctuations are related to the currents of each three-phase line, performing transformations to the variables to find optimal settings. The second methodology is a graphical analysis of the frequency spectra obtained with the Fourier transformation for the pressure fluctuation, vibrations, torque, triphasic currents, and voltages.

2. METHODOLOGY

2.1 Process Design

The hydraulics laboratory of the EAFIT University located in Medellín, Colombia is used to perform all the measurements for this work. The scheme of the equipment used is shown in Fig. 1. This scheme is composed of two centrifugal pumps in series with electric motors (2 hp for the ITT-Goulds stainless steel 316 and 3 Hp for the recirculation pump) and each pump has six blades. The test bench is composed of a closed piping system with a water reservoir (Bolaños and Botero 2021). Measurement instruments include an accelerometer, tachometer, flow meter, torque sensor, and thermometers.

Table 1 Specifications elements of the practice.

Impeller	
External diameter	0.14764 m
Reference diameter	0.08104 m
Number of blades (backward curved)	6
Inlet and outlet pipes	
Inlet diameter (suction hole)	0.0635 m
Outlet diameter (discharge hole)	0.0508 m
Design specifications	
Flow	0.009 m ³ /s
Head	7.7 m
Mechanical power	1118.5 W
Electric motor	
Power	2 hp
Speed	1745 rpm
Phases	3
Stream	5.6 - 5.2/2.6 A
Voltage	208 - 230 / 460 V
Frequency	60 Hz

Turbollogger is a data processing software developed in a LabView® environment by researchers from EAFIT University and is successfully used in different applications in academic and mechanical industries (Bolaños and Botero 2021).

Two types of measurement campaigns are done. In the first campaign, the 2 HP motor works in turbine mode. For the second campaign, the study pump is placed in pump mode. Angular velocity ranges from 700 rpm to 1900 rpm in ascent and descent is used. Table 1 shows the specifications of the system elements. The pump under study is operated in a speed range between 700 to 1700 rpm in pump mode and from 700 to 1900 rpm in turbine mode. The different rotation speeds are obtained with a speed variator (Bolaños and Botero 2021).

2.2 Instrumentation and data acquisition

Table 2 shows the instrumentation used for the

Table 2 Specifications measuring instruments and their uncertainties (Bolaños and Botero 2021).

Instrument	RO (Rated Output)	Intervals	Span	Linearity	Repeatability	Hysteresis	Sensitivity
Dytran 2005V	0 - 5 VDC	0 - 50 psi	344738 Pa	±0.1 % of span	-	-	100 mV/psi
Kistler 8704B50M1	±5 V	±50 g	100 g	±1 % of RO	-	-	100 mV/g
Futek TRS600 FSH01998	±5 VDC	-20 - 20 Nm	40 Nm	±0.2 % of RO	±0.2 % of RO	±0.1 % of RO	-
GE TransPort PT878	4 - 20 mA	-10 l/s - 20 l/s	30 l/s	-	±0.1% a ±0.3%	-	-
DT2234C+	0 - 5 V	2.5 - 99999 rpm	99996.5 rpm	-	-	-	0.1 rpm (2.5 - 999.9 rpm) 1 rpm (1000 - 99999)

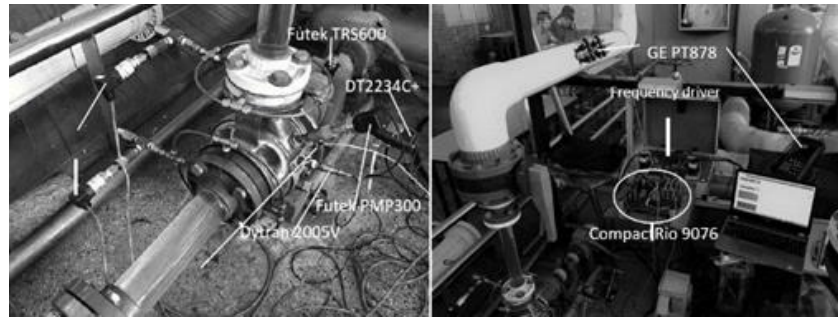


Fig. 2. Location of measuring instruments (Bolaños and Botero 2021).

measurement campaigns and the main technical characteristics of the instruments. Notation RO of this Table indicates Rated Output (RO). Figure 2 illustrates the location of the measurement instruments in the equipment. The following measurements are performed to relate hydraulic and electrical variables: Dytran 2005V piezoelectric pressure transducer for measuring pressure fluctuations in the volute; Kistler 8704B50M1 accelerometer installed in the volute; Futek TRS600 FSH01998 torque sensor placed on the pump shaft; General Electric (GE) TransPort PT878 ultrasonic flow meter mounted on the 6" pipe to the high-pressure area; conventional digital tachometer DT2234C+ to measure the speed of the pump on the shaft. This tachometer is modified to send voltage signals to data acquisition equipment. The sensitivity analysis is presented in Table 2 and corresponds to the sensitivity of the unmodified equipment.

Electrical signals transmitted by sensors are received and processed using National Instruments® CompactRio® 9076 data acquisition equipment and the Turbologger software. The data acquisition equipment is made up of two acquisition modules, NI-9232 and NI-9203, and there are three different groups for data acquisition. All signals are recorded simultaneously. Group 0 is based on a Hydromechanical – 9232 and contains the dynamic signals of hydraulic and mechanical origin, acquired with the NI9232 module: pressure fluctuations, accelerometer, and torque. Group 1 is based on hydraulics - 9203: Contains stochastic signals of hydraulic origin (independent of time), acquired with the NI9203 module: Gauge pressures (high and low), flow rate, fluid temperature, and engine temperature. Group 2 contains dynamic signals of electrical origin: voltages and currents of the different phases.

2.3. Characteristic Curves

Centrifugal pumps can work under different operating conditions, transient states such as starting or stopping changes in fluid direction, or changes in rotation. It is precisely this possibility of inverting the rotation or the flow that allows the operation in turbine mode (Bolaños 2018). This diversity of operation modes that centrifugal pumps present makes it necessary to have a complete characterization tool that allows identifying all the operating zones of the machine and its efficiency in each one of them. This tool is the characteristic curves of four quadrants. Characteristic curves are

graphical representations of the behavior of turbomachines with respect to variables of interest such as angular speed, flow rate, torque, and power, among others (Bolaños 2018; Bolaños and Botero 2018).

One of the advantages of the characteristic curves is the representation in a single graph of the behavior of all the possible operating points of a turbomachine. The four quadrants I, II, III, and IV correspond to the modes of operation: pump, brake pump, turbine, and reverse rotation pump, respectively. The characteristic curves also help to identify problem areas that may be associated with the presence of hydrodynamic phenomena. These zones are normally found where there are changes in the sign of slope in the characteristic curves (Bolaños 2018; Bolaños and Botero 2018).

For the pump under study, measurements are taken in the operating modes such as pump and turbine. In this work, three are the criteria selection of the pump and turbine operating conditions. Firstly, there must be a correspondence between the desired quadrants of the pump and turbine modes. Secondly, a cleaning process of the sample of those points that presented noise in the measurements. Thirdly, the operating points whose graphs are clearer and showed better amplitude peaks in the variables chosen. In each of the operating modes, records of the sensors are taken, varying the angular speed of the 2 Hp pump and maintaining a fixed frequency of 60 Hz. Initially from low to high rpm (climb), and later from high to low rpm (decline), these variations are made in 100 rpm intervals. Both modes of operation are done with an angular speed of 1700 rpm for the pump study. However, for the pump mode, the speed of the recirculation is around 1100 rpm and for the turbine mode, the speed is around 1900 rpm.

2.4. Couple Analysis

A copula is a function that relates a multivariate distribution with its one-dimensional marginal distribution functions, regardless of the shape or type of the marginal distributions (Gómez 2017). This method is used in this work to develop a predictive statistical model in order to relate the hydraulic variables with non-invasive variables (electrical variables). If $H(x,y)$ is a joint distribution function of two continuous variables, then a copula C can be defined that relates the marginal distributions F and G of the random variables x and y in the way shown

in Eq. 1 and for the case where the variables are independent, it can be modeled using the copula $C(x,y)=xy$ (Taillon *et al.* 2019). $F(x)$ and $G(y)$ are the marginal distributions for each of the physical variables and in this case a hydraulic variable and an electrical variable.

$$H(x, y) = C(F(x), G(y)) \quad (1)$$

2.5. Spectral Analysis

The power density spectra using the Fourier transform for the fluctuating variables pressure, vibrations, currents, and voltages are plotted. Spectra for the 1.4x, 4x, and 25x domains are plotted, using logarithmic scales on the required axis. The most outstanding amplitude peaks are marked. The spectral analysis is done using Python-free software.

3. RESULTS AND DISCUSSIONS

The analysis is presented in two parts. The first is based on a statistical analysis of the information obtained, and the second is based on a graphic analysis of the frequency spectra for each of the variables under study and provides a predictive statistical model. The variables for analysis are the Dytran (the pressure fluctuations in the volute) in Volts (V), the accelerometer (the vibrations) in m/s², the shaft torque in Nm, Current 1 to 3 in amperes (A), and Voltage 1 to 3 in Volts (V).

Firstly, the authors have done a fitting procedure to find linear regression to explain the relationship between the electrical variables and the hydraulic variables or vice versa. When the fitting procedure is done, the determination coefficient (R^2) is around 0.0005 with a p-value of 0.001. Also, the p-values of the current 1 to 3 are below 0.82. The above indicated that there is no statistical significance and the R^2 does not describe properly the linear model proposed (Bolaños 2018; Taillon *et al.* 2019; Bolaños and Botero 2021). An alternative to describe this phenomenon is a non-linear adjustment using copula analyses. This copula analysis requires the adjustment of the marginal distributions of the variables under study. In this order of ideas, the predictive statistical model is done by copulas and the procedure for development includes (i) adjustment of marginal distributions; (ii) Box-Cox transformation; (iii) Johnson transformation; (iv) Copula adjustment and (v) Graphical analysis of spectra, and these methodological steps are explained as follows.

3.1 Adjustment of Marginal Distributions

Arena software is used to fit the marginal probability distributions for each variable, particularly the input analyzer tool. The available probability distributions are fitted, and the Kolmogorov-Smirnov (KS) and chi-square tests are performed. Also, transformations are made to each variable to seek better results, including the square root of each variable, the natural logarithm, and a new variable called currents which

can be seen in Eq. (2). In the appendix (Tables 1A and 2A) shows the KS test of the studied variables (Dytran, Current 1 to 3, RootCurrent 1 to 3, LnCurrent 1 to 3, and the general current) where Table 1A is related to the p-values of the KS test for each test performed in pump mode and Table 2A shows them for the turbine mode. As can be seen in these Tables the p-values of the chi-square test are less than 0.005. Also, with a common significance level of 0.05 can be concluded that no statistical evidence that the evaluated variables or transformations can fit the different probability distributions. In the case of the Dytran variable, an attempt could be made to adjust to a Beta or normal distribution for another significance level lower than the p-level shown.

$$\begin{aligned} \text{Current} \\ = \sqrt{\text{Current } 1^2 + \text{Current } 2^2 + \text{Current } 3^2} \end{aligned} \quad (2)$$

Graphical analysis is performed to observe that the Dytran variable can be modeled using normal probability distribution to find possible adjustments and different transformations for the rest of the variables. Figures. 1A and 2A provided in the appendix show the frequency histograms of each study variable in each mode of operation. In the case of the Dytran variable and the Current variable, can be noted that the histogram is approximately symmetric and has a slight Gaussian bell shape. The authors decided to adjust the Dytran variable to a normal distribution and for the Current variable a Box-Cox transformation which is possible since all its values are positive. The Johnson transformation (Lagos and Vargas 2003) is also performed for each of the currents and the current variable since the transformation can be done with positive and negative values.

3.1.1. Box Cox Transformation

The Box-Cox potential transformation is used to correct biases in the distribution of errors, unequal variances, and mainly non-linearity. Eq. (3) shows the normal distribution of the data formula used. In this equation the value of lambda (λ) used is obtained from the maximization of Eq. (4), where n corresponds to the number of observations, x_i is the observation, y_i is the transformation, μ and σ^2 is the average and variance of the transformations, respectively (Li 2005). Also, the lambda value varies between -5 and 5.

The results of the fit to the normal distribution of the Box-Cox transformation (b_c) for the pump and turbine modes are applied only to positive values, i.e., it is performed only on the current variable (Eq. (2)). The results of this processes indicated that the transformation carried out on the data still does not pass the normality criterion since its p-values do not offer statistical significance as can be seen in Table 3A of the appendix.

$$y(\lambda) = \begin{cases} \frac{y^\lambda - 1}{\lambda}, & \lambda \neq 0 \\ \log y, & \lambda = 0 \end{cases} \quad (3)$$

$$\log[L(\lambda, \mu, \sigma)] = \frac{-n}{2} \log(2\pi) - \frac{n}{2} \log(\sigma^2) - \frac{1}{2\sigma^2} \sum_{i=1}^n (y_i - \mu)^2 + (\lambda - 1) \sum_{i=1}^n \log(x_i) \quad (4)$$

Table 3 Johnson transformations

Johnson transformation	Equation
SB	$Z = \gamma + \eta \ln\left(\frac{X - \epsilon}{\lambda + \epsilon - X}\right)$
SL	$Z = \gamma + \eta \ln(X - \epsilon)$
SU	$Z = \gamma + \eta \sinh^{-1}\left(\frac{X - \epsilon}{\lambda}\right)$

3.1.2. Johnson Transformation

Another technique for transforming non-normal data into normal data is the Johnson Distribution Families system. Table 3 shows the mathematical models for the Johnson transformation related to the SB (refers to bounded random variable X), SL (refers to X bounded below or lognormal), and SU (refers to unbounded X) (Lagos and Vargas 2003). R statistical package is used, particularly the Johnson library is applied to fit the data and to determine the type of family of the transformation. Table 4 shows the parameters for each variable according to each transformation performed.

In the case of the pump mode, the current variable has a p-value greater than a significance level of 0.05, which indicates that there is statistical evidence to not rule out the normality hypothesis. Figure 3 shows the histograms for each transformation. Johnson and the Gaussian bell shape can be corroborated for the current variable in pump mode. For the case of the turbine mode, the p-value is 0.01 with the KS test. Figure 4 shows the histograms for the Johnson transformations in the turbine mode, where the approximate Gaussian bell shape of the current's variable in this mode of operation can be shown.

Table 4 Johnson transformation parameters performed by variable in each operation mode

Johnson transformation								
	Pump mode				Turbine mode			
	Current1	Current2	Current3	Current	Current1	Current2	Current3	Current
Family	SB	SB	SB	SU	SB	SB	SB	SU
Gamma, γ	-0.01	-0.03	-0.02	-0.88	-0.06	0.01	-0.07	-0.43
Lambda, λ	13.16	13.06	13.32	3.79	12.21	12.33	12.82	4.06
Epsilon, ϵ	-6.62	-6.58	-6.73	5.35	-6.24	-6.22	-6.57	4.08
Eta, η	0.64	0.61	0.64	3.82	0.87	0.85	0.90	3.42
p-value of KS	0.00	0.02	0.06	0.03	0.00	0.00	0.01	0.01

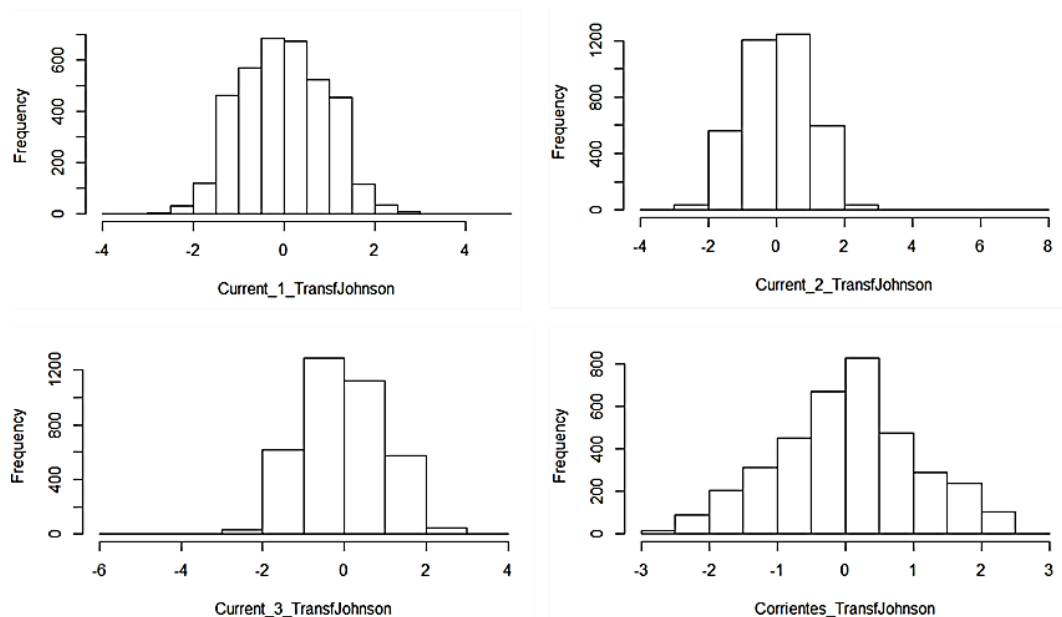


Fig. 3. Histograms for Johnson transformations in pump mode.

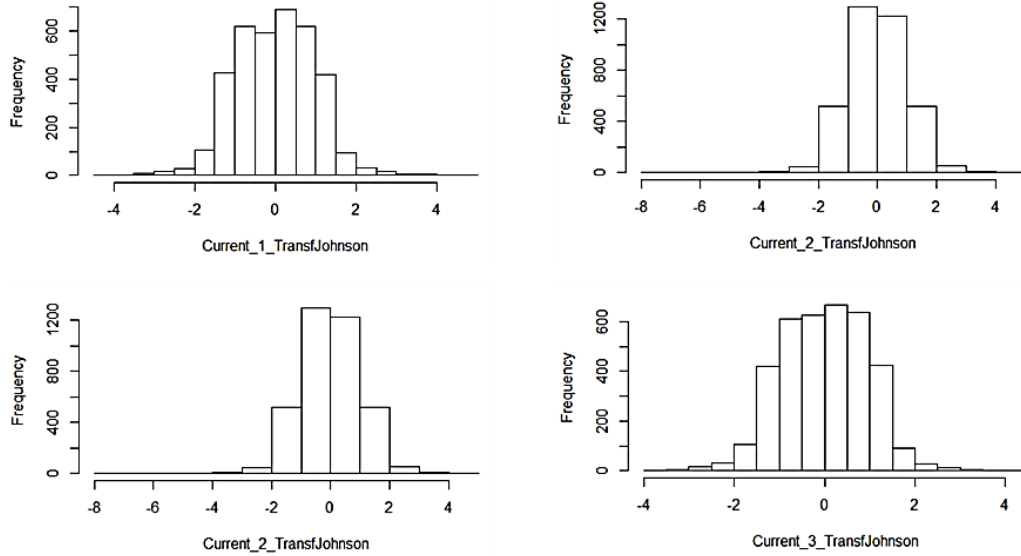


Fig. 4. Histograms for Johnson transformations in turbine mode.

For the other analysis, a normal distribution fit is applied for the current variable in the two modes of operation of the machine under study. In the pump mode, for the Dytran variable, a normal distribution with a mean of 0.00106 and a standard deviation of 0.0027 is fitted. For the current variable that has been transformed with the Johnson model, a normal distribution with a mean of 0.0225 and a standard deviation of 1.03 is obtained. In the turbine mode, for the Dytran variable, there is a normal distribution with a mean of -0.0021 and a standard deviation of 0.0053 and for the current variable transformed with Johnson there is a normal distribution with a mean of 0.026 and a standard deviation of 1.03.

Once the variables are analyzed and each of their marginal distributions is defined, the fit for the Dytran and currents variables is found using the VineCopula and VC2copula copula packages of the R software.

3.2. Copula Adjustment

For the pump mode, a better fit is obtained with the type 2 Tawn copula whose cumulative distribution function is defined by Eq. 5 and whose generating function is shown in Eq. 6, where u and v correspond to the evaluation of the marginal distributions of each variable (Jaramillo-Elorza and Lozano 2014).

$$C(u, v) = (u * v)^{A(w)}, \text{ where } w = \frac{\ln(u)}{\ln(u * v)} \quad (5)$$

$$A(t) = (1 - \psi_2)(1 - t) + (1 - \psi_1)t + [\psi_1(1 - t)^\theta + (\psi_2 t)^\theta]^{\frac{1}{\theta}} \quad (6)$$

With copula parameters $t \in [0, 1], 0 \leq \psi_1, \psi_2 \leq 1$ and $\theta \in [1, \infty]$. There can be two classes of Tawn copulas

Table 5 Adjustment parameters of the Tawn Copula type 2 for pump mode.

Parameter	Value
ψ_1	0,01
ψ_2	1
θ	2.44
p-value	0.03
AIC	-8.09

(type 1 and 2), and this refers to the value that the asymmetric parameter ψ can be assumed ($\psi_1 = 1$ or $\psi_2 = 1$) (Lagos and Vargas 2003). Table 5 shows the p-value of the independence test and it may suggest that the hypothesis of independence of the variables is accepted. The Akaike Information Criterion (AIC) is presented, whose logic of comparison between adjustment of copulas is to choose the one with the lowest value (Genest and Favre 2007). Figure 5 shows the suggested copula density function.

Chi-plot and K-plot are made to represent a graphical behavior of the possible functional dependence of two random variables. Figure 3A and Fig. 4A

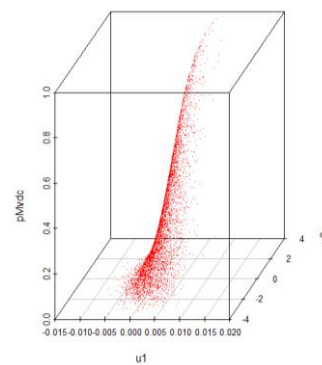


Fig. 5. Density graph for the fit of the Tawn Copula type 2 for pump mode.

presented in the appendix show the Chi-plot and K-plot graphs for the proposed adjustment. As can be seen in both cases, the criteria of the graphic analysis are met to define the dependence of the variables. In the case of the K-plot graph, positive functional dependence is detected by accentuating the concavity of the point cloud with respect to the diagonal, when the variables are independent the graph is concentrated on the diagonal (Moreno 2012). Also, Fig. 5A shows the comparison of the copula fit with the observed data, showing a greater relationship in the central part of the variables.

For the turbine mode, the fitted results showed independence. This is one of the simplest models since they assume independence between all the variables, i.e., it is assumed that the joint probability distribution can be represented as the product of the univariate and independent probability distributions as indicated in Eq. 7 (Flórez and Jiménez 2008). The p-value for independence is 0.73 and the AIC = 0.

$$C(F(x), G(y)) = F(x) * G(y) \quad (7)$$

3.3. Graphic analysis of Spectra

3.3.1. Pump Mode

Figure 6 shows an analysis of the Time Synchronous Average (TSA). In this figure, the blue lines indicate a nominal value of the pressure variation in the sensor measurement, and the red lines show the 95 % confidence interval of the measurement. The polar graph for the point of operation in pump mode shows that, despite being the point of higher efficiency of the measurements, the turbomachine presents slightly unbalanced flows, and these could be reflected in rotodynamic, or other forces transferred from the shaft to the rotor.

Spectral graphs are made for each of the hydraulic and electrical variables selected in this work. The

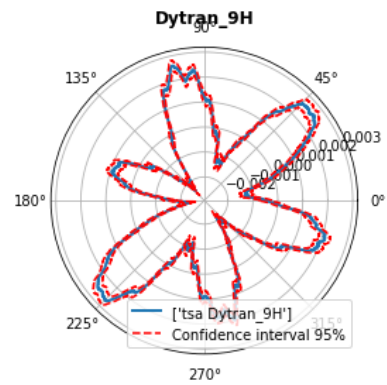


Fig. 6. Polar graph for the Dytran variable in pump mode.

aim is to find those points where the information has been transferred from the hydraulic part to the electrical variables of current or voltage. Figure 7 shows the power density spectra for the Dytran variable. Also, in the appendix can be found the Fig. 6A related to the accelerometer variable, and Fig. 7A for the torque in the 1.4x, 4x, and 25x frequency domains, and the peaks of higher amplitudes. The frequency domain is normalized using the rotational speed of the turbomachine as a reference, obtaining the horizontal axis of orders of the rotational frequency of the machine.

The amplitude peaks at frequencies 0.58x, 0.8x, 1x, 2x, 3x, 3.4x, 4.9x, 5.4x, and 6x are common in these figures and the last peak corresponds to the step of blades. The information has moved from the volute and the casing to the turbomachine shaft, i.e., the pressure fluctuations cause the casing to vibrate, and these fluctuations and vibrations cause changes in torque, or it could also be seen in the opposite direction where the changes in torque have caused the vibrations in the casing and the pressure fluctuations registered in the volute.

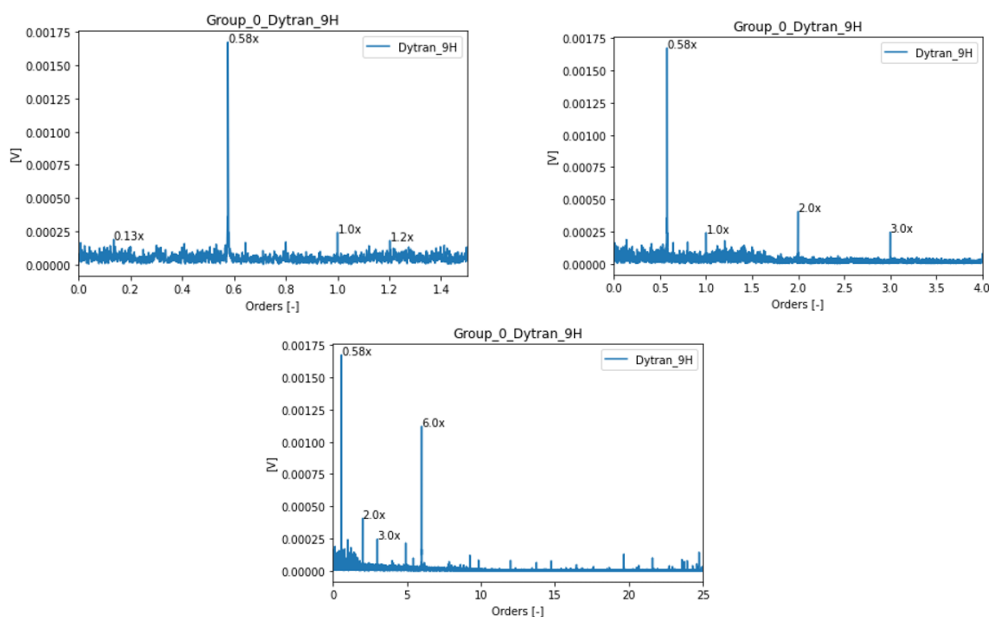


Fig. 7. Spectra for the Dytran variable in pump mode.

For the case of currents, the frequency spectra are shown in Fig. 16A for a frequency of 25x. As can be seen in the figure, the amplitudes have significantly small dimensions compared to the other variables. The spectra are made at the 1.4x and 4x frequencies with logarithmic scales on the vertical axis and are shown for the currents in Fig. 17A provided in the appendix.

For the comparison between the peaks of the variables Dytran, accelerometer, Torque, currents and voltages, the creation of an upper limit (LS) is proposed that will indicate when the amplitude peak would correspond to atypical data. This limit is established according to Eq. 8, where μ and σ are the mean and standard deviation of each variable and the parameter k corresponds to the number of deviations considered with respect to the standard deviation of the sample.

For the case of the three currents $k = 1$ is established and for the rest of the variables $k = 1.5$ since it is observed that in the case of the electrical variables the data are more concentrated on the central value or the mean and for the rest of the variables it is desired to obtain those that are much further away from said central value. It is also tested with a lower limit, but none of the data is below the resulting value.

$$LS = \mu + k\sigma \quad (8)$$

The results of those values that exceed the established upper limits are shown in Table 4A for the subsynchronous region and in Table 5A for the rest of the scale. D-A-T corresponds to those amplitude peaks that are common between the Dytran, Accelerometer and Torque variables. D-A corresponds to the common peaks between Dytran and the accelerometer. D-T corresponds to the common peaks between Dytran and Torque. Box I refer to the amplitude values where the current 1, 2, and 3 exceeded the LS value.

As can be seen, the Dytran and Accelerometer variables have the highest number of peaks in common, which can give an idea of how the fluid information is also transmitted to the casing. The peak shown on the 2.4x scale for D-T is very close to the peak of the currents at the 2.5x scale, as well as for the 8.3x and 20.8x scales when compared to 7.8x and 19.7x for D-A. In the subsynchronous scale no peaks in the currents are appreciated. Although there are no data in the currents that exceed the LS value, there are two representative peaks in the 0.75x and 0.88x domains that are equal to the common D-A-T peaks. In the case of voltages, Fig. 10A shows the spectra for this variable. Significant peaks are obtained at the 12.5x and 13.2x scales, which are very close to the D-A peaks at 12 and 14.7x.

3.3.2. Turbine mode

Figure 8 shows the polar graph for the point of operation in turbine mode. Similar to the notation lines in Fig. 6, the blue lines indicate a nominal value

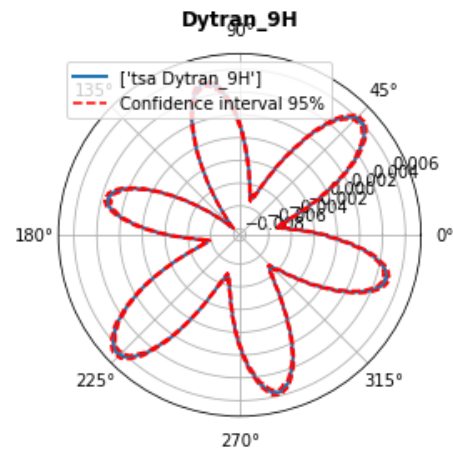


Fig. 8. Polar graph for the Dytran variable in turbine mode.

of the pressure variation in the sensor measurement, and the red lines show the 95 % confidence interval of the measurement. The turbomachine still shows slightly unbalanced flows, however to a lesser extent in this mode of operation. The power density spectra are made and are shown in Fig. 9 for the Dytran variable. Also, in Fig. 11A for the accelerometer variable and Fig. 12A for the torque in the 1.4x, 4x, and 25x scales with the highest amplitude elevated peaks marked.

In a quick observation, the 1x, 2x and 6x peaks are common for the three graphs of the Dytran, accelerometer and torque variables. This may be an indication that the information has been transferred from the volute, the casing up to the axis of the turbomachine. Thus, the pressure fluctuations cause the casing to vibrate, and these fluctuations and vibrations cause changes in torque. It could also be interpreted in the opposite direction where the changes in torque caused the vibrations in the casing and pressure fluctuations recorded in the volute.

For the case of currents, the frequency spectra are shown in Fig. 10 for a 25x scale. This figure is made in the x-axis with a logarithmic scale in order to have a better visualization, however, the y-axis represents the current in Amperes, and this measurement is not transformed. As can be seen, the amplitudes have significantly small dimensions compared to the other variables. Figure 11 shows the spectra that are made at 1.4x and 4x scales with logarithmic scales on the vertical axis for the currents.

For the comparison between the peaks of the variables, Dytran, accelerometer, Torque, currents, and voltages in turbine mode, the creation of an upper limit (LS) of Eq. (8) is also proposed. For the case of the three currents $k = 1$, and for the rest of the variables $k = 1.5$ since it is observed that in the turbine mode in the electrical variables the data is more concentrated on the central value or the mean and for the rest of the variables it is desired to obtain those that move much further away from that central value. It is tested again with a lower limit, but none of the data is below the resulting value.

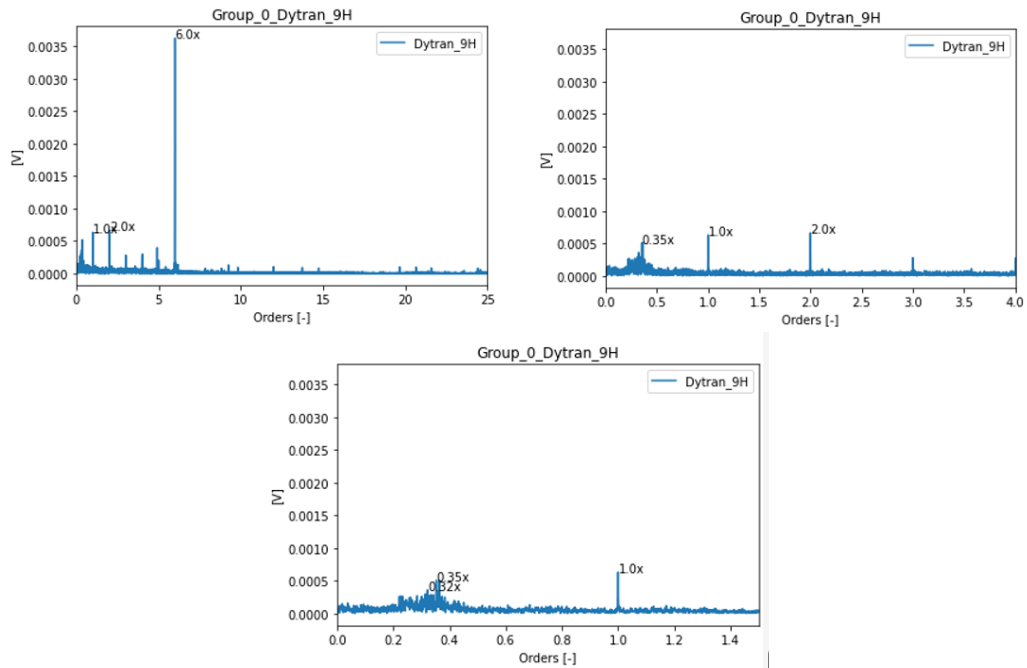


Fig. 9. Spectra for the Dytran variable in turbine mode.

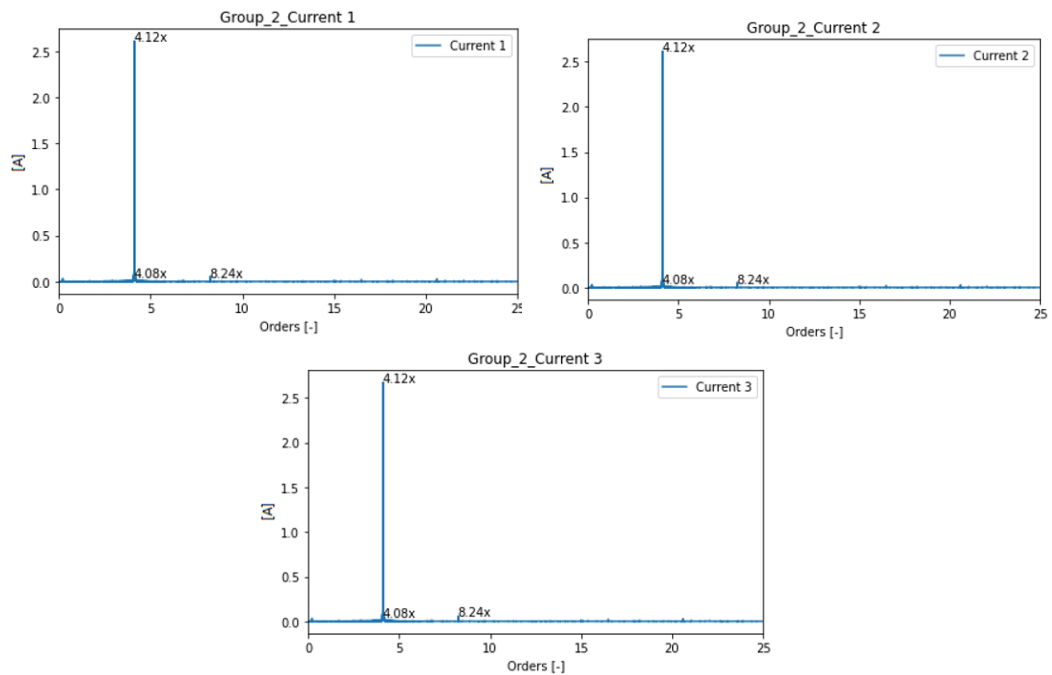


Fig. 10. Spectra for currents in turbine mode.

The results of those values that exceed the established upper limits are shown in Table 6A for the subsynchronous region and in Table 7A for the rest of the scale. The Dytran and Torque variables have the highest number of peaks in common, this reflects the pump's operating mode as a turbine since now the motor behaves as a generator. Likewise, there is a significant number of peaks in common between the Dytran variable and the accelerometer, which continues to show the flow of information between the fluid and the casing.

In the subsynchronous region, the information reached each of the elements and there is a point of great interest in the 0.2x scale since a common peak is presented between Dytran, Torque, and the three currents and it is located in the subsynchronous region. Another common amplitude peak is the one located at 8.2x between the Dytran, the accelerometer, and the three currents. Additionally, there is a common peak shown in Fig. 11 in the 1.6x domain for the currents and D-T. For the case of voltage, Fig. 13A shows the spectra for the three voltages, peaks 12.2 and 13.1 are very close to 12 and 13.7 of D-T.

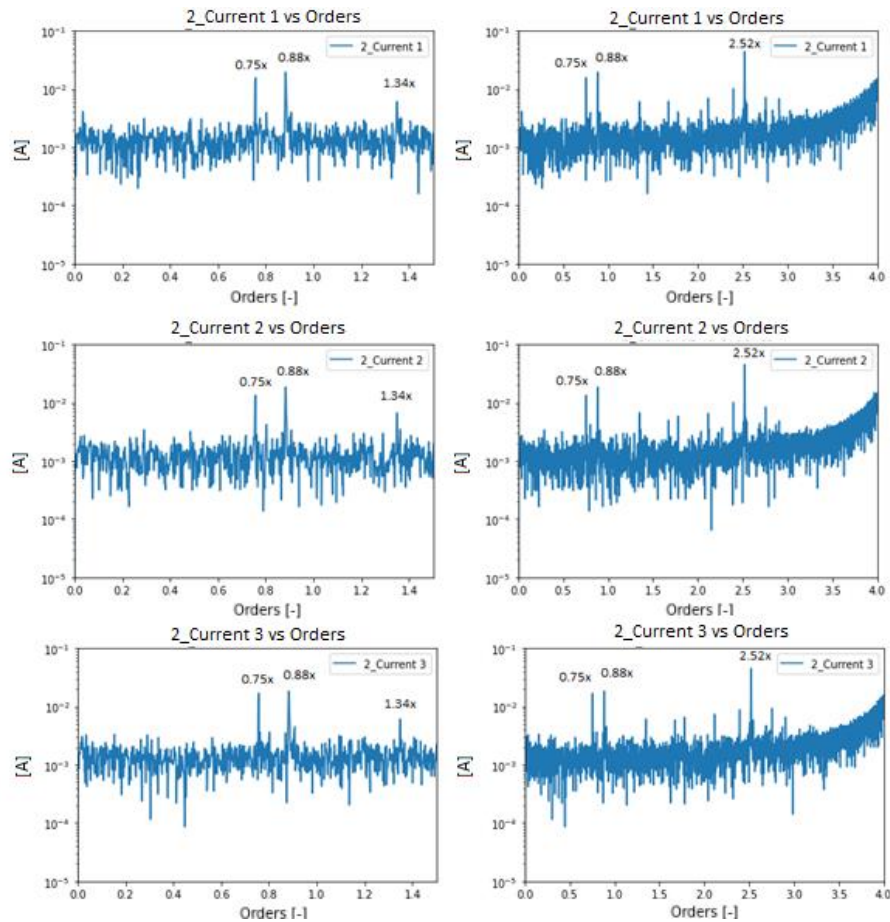


Fig. 11. Spectra for the currents in logarithmic scale for the turbine mode.

5. CONCLUSION

The following conclusions and recommendations can be drawn.

This work aims to do an analysis of the frequency spectrum of the electrical variables (non-invasive variables) in order to provide information on the hydraulic variables using graphical and statistical analysis. In order of ideas, the authors do a predictive model using a joint probability distribution from the electrical and hydraulic marginal variables.

In the pump and turbine modes, a statistical analysis is performed. Non-significant statistical evidence at a 95 % confidence level is found for the adjustment to a common probability distribution of the pressure fluctuation variables related to the three currents, and the three voltages of the three-phase network.

In the pump mode, the dependence of the variables is observed with a p-value of around 0.03. An adjustment to a proposed copula is obtained that corresponds to a Tawn type 2, with an AIC value of around -8.09. The fit is achieved with the product of the marginal values of each variable.

The spectra analysis for the pump mode show common peaks are observed among each of them, i.e. there are points where the information has been transferred from the volute, the casing to the axis.

Nevertheless, there are close points between the amplitude peaks of the currents and the voltages, which give an indication that the information has been able to reach the electrical terms.

For the turbine mode in the spectral analysis, there is a common point between all the study variables and peaks, i.e. the information has been transferred to or from the electrical terms.

Further works are needed to develop other predictive models that use copulas in order to describe hydraulic variables with electrical variables, for example, single-variable or multivariate control charts (Aas *et al.* 2021). Also, statistical curves or tables that relate electrical or hydraulic variables can be developed and will be used for industrial applications (Liu *et al.* 2021).

ACKNOWLEDGEMENTS

The authors are grateful for the support of each institution during the present work.

REFERENCES

- Aas, K., T. Nagler, M. Jullum and A. Løland (2021). Explaining predictive models using shapley values and non-parametric vine copulas. *Dependence Modeling* 9(1), 62-81.

- Al-Hashmi, S. A. (2012). Spectrum analysis of acoustic signals for cavitation detection. In *IEEE Symposium on Industrial Electronics and Applications*, Bandung, Indonesia.
- Al-Obaidi, A. R. (2019). Investigation of effect of pump rotational speed on performance and detection of cavitation within a centrifugal pump using vibration analysis. *Heliyon* 5(6), e01910.
- Baldassarre, A., M. De Lucia and P. Nesi (1998). Real-time detection of cavitation for hydraulic turbomachines. *Real-Time Imaging* 4(6), 403-416.
- Bolaños, H. D. (2018). *Fenómenos Hidrodinámicos Periódicos en Una Bomba Centrífuga de Baja Velocidad Específica*. Bachelor's thesis, EAFIT University, Medellín, Colombia.
- Bolaños, H. D. and F. Botero (2021). Four-quadrant Characterization of hydrodynamic phenomena in a low specific speed centrifugal pump. *Ingeniería y Universidad* 25, 1-22.
- Bolaños, H., G. Angarita, S. Richard and F. Botero (2019). Image processing in vortex rope characterization. *Revista Colombiana de Tecnologías de Avanzada* 3, 101-108.
- Flórez, R. O. and J. A. Jiménez (2008). Máquinas hidráulicas reversibles aplicadas a micro centrales hidroeléctricas. *IEEE Latín América Transactions* 6(2), 170-175.
- Genest, C. and A. C. Favre (2007). Everything you always wanted to know about copula modeling but were afraid to ask. *Journal of Hydrologic Engineering* 12(4), 347-368.
- Gómez Ríos, W. J. (2017). *Análisis de Frecuencia Hidrológico Multivariado Para Eventos Extremos Mediante Funciones Cópula Arquimedianas. Casos de Estudio: Cuenca Baja Del Río Tunjuelo Y Región De La Mojana (Colombia)*. Master thesis, Universidad Nacional de Colombia, Bogotá, Colombia.
- Jaramillo-Elorza, M. C. and J. A. Lozano (2014). Construcción de distribuciones multivariadas con marginales dependientes usando cópulas en R. *Ciencia en Desarrollo* 5(1), 21-29.
- Lagos, I. J. and J. A. Vargas (2003). Sistema de familias de distribuciones de Johnson, una alternativa para el manejo de datos no normales en cartas de control. *Revista Colombiana de Estadística* 26(1), 25-40.
- Li, G., X. Ding, Y. Wu, S. Wang, D. Li, W. Yu, Y. Zhu and Y. Guo (2022). Liquid-vapor two-phase flow in centrifugal pump: Cavitation, mass transfer, and impeller structure optimization. *Vacuum* 201, 111102.
- Li, P. (2005). Box-Cox transformations: an overview. Presentation. <https://www.ime.usp.br/~abe/lista/pdfm9cJKUmFZp.pdf>.
- Liu, D., C. Li and O. P. Malik (2021). Nonlinear modeling and multi-scale damping characteristics of hydro-turbine regulation systems under complex variable hydraulic and electrical network structures. *Applied Energy* 293, 116949.
- Machado, G., E. Albáñez, J. Rengifo and A. Bueno (2016). Diagnóstico de cavitación en bombas centrífugas mediante técnicas espectrales no invasivas. In *13th International Congress on Numerical Methods in Engineering and Applied Sciences*, Rome, Italy.
- Moreno, D. C. (2012). *Method to Choose an Archimedean Copula Optimal*. Ph. D. thesis, Universidad Nacional de Colombia, Bogotá, Colombia.
- Mousmoulis, G., J. Anagnostopoulos and D. Papantonis (2019). A review of experimental detection methods of cavitation in centrifugal pumps and inducers. *International Journal of Fluid Machinery and Systems* 12(1), 71-88.
- Muttalli, R. S., S. Agrawal and H. Warudkar (2014). CFD simulation of centrifugal pump impeller using ANSYS-CFX. *International Journal of Innovative Research in Science, Engineering and Technology* 3(8), 15553-15561.
- Obidov, B., O. Vokhidov, D. Tadjieva, D. Saidkhodjaeva, U. Kurbanova and A. Isakov (2021). Hydrodynamic effects on the flow elements of the downstream devices in the presence of cavitation. In *IOP Conference Series: Materials Science and Engineering*, Tashkent, Uzbekistan.
- Perez, R. X (2022). *Evaluating Centrifugal Pumps in Petrochemical Applications. Maintenance, Reliability and Troubleshooting in Rotating Machinery*. John Wiley and Sons, New Jersey, USA.
- Taillon, G., K. Onishi, T. Mineshima and K. Miyagawa (2019). Statistical analysis of cavitation erosion impacts in a vibratory apparatus with copulas. *IOP Conference Series: Earth and Environmental Science* 240(6), 062035.
- Ullum, U., J. Wright, O. Dayi, A. Eceder, A. Soulaïmani, R. Piché and H. Kamath (2006). Prediction of rotating stall within an impeller of a centrifugal pump based on spectral analysis of pressure and velocity data. *Journal of Physics: Conference Series* 52(1), 36-45.
- Wang, Y., X. Wang, J. Chen, G. Li, H. Liu and W. Xiong (2022). An experimental insight into dynamic characteristics and wear of centrifugal pump handling multi-size particulate slurry. *Engineering Failure Analysis* 138, 106303.

APPENDIX A

Table 1A Marginal distributions fit for pump mode.

	Beta	Normal	Erlang	Gamma	Lognormal	Weibull	Triangular	Uniform	Exponential
Dytran	0.0137	0.0222	<0.01	<0.01	<0.01	<0.01	<0.01	<0.01	<0.01
Current 1	<0.01	<0.01	<0.01	<0.01	<0.01	<0.01	<0.01	<0.01	<0.01
Current 2	<0.01	<0.01	<0.01	<0.01	<0.01	<0.01	<0.01	<0.01	<0.01
Current 3	<0.01	<0.01	<0.01	<0.01	<0.01	<0.01	<0.01	<0.01	<0.01
RaizCurrent 1	<0.01	<0.01	<0.01	<0.01	<0.01	<0.01	<0.01	<0.01	<0.01
RaizCurrent 2	<0.01	<0.01	<0.01	<0.01	<0.01	<0.01	<0.01	<0.01	<0.01
RaizCurrent 3	<0.01	<0.01	<0.01	<0.01	<0.01	<0.01	<0.01	<0.01	<0.01
LnCurrent 1	<0.01	<0.01	<0.01	<0.01	<0.01	<0.01	<0.01	<0.01	<0.01
LnCurrent 2	<0.01	<0.01	<0.01	<0.01	<0.01	<0.01	<0.01	<0.01	<0.01
LnCurrent 3	<0.01	<0.01	<0.01	<0.01	<0.01	<0.01	<0.01	<0.01	<0.01
Current	<0.01	<0.01	<0.01	<0.01	<0.01	<0.01	<0.01	<0.01	<0.01

Table 2A Fit of marginal distributions for turbine mode.

	Beta	Normal	Erlang	Gamma	Lognormal	Weibull	Triangular	Uniform	Exponential
Dytran	0.0137	<0.01	<0.01	<0.01	<0.01	<0.01	<0.01	<0.01	<0.01
Current 1	<0.01	<0.01	<0.01	<0.01	<0.01	<0.01	<0.01	<0.01	<0.01
Current 2	<0.01	<0.01	<0.01	<0.01	<0.01	<0.01	<0.01	<0.01	<0.01
Current 3	<0.01	<0.01	<0.01	<0.01	<0.01	<0.01	<0.01	<0.01	<0.01
RaizCurrent 1	<0.01	<0.01	<0.01	<0.01	<0.01	<0.01	<0.01	<0.01	<0.01
RaizCurrent 2	<0.01	<0.01	<0.01	<0.01	<0.01	<0.01	<0.01	<0.01	<0.01
RaizCurrent 3	<0.01	<0.01	<0.01	<0.01	<0.01	<0.01	<0.01	<0.01	<0.01
LnCurrent 1	<0.01	<0.01	<0.01	<0.01	<0.01	<0.01	<0.01	<0.01	<0.01
LnCurrent 2	<0.01	<0.01	<0.01	<0.01	<0.01	<0.01	<0.01	<0.01	<0.01
LnCurrent 3	<0.01	<0.01	<0.01	<0.01	<0.01	<0.01	<0.01	<0.01	<0.01
Current	<0.01	<0.01	<0.01	<0.01	<0.01	<0.01	<0.01	<0.01	<0.01

Table 3A Box Cox transformation of the current variable for pump and turbine modes.

Transformation	Error	p-value of KS	p-value of Chi squared
Transf_bc_bomb	0.00139	<0.005	<0.01
Transf_bc_turb	0.00172	<0.005	<0.01

Table 4A Amplitude peaks exceeding LS in the subsynchronous region in pump mode.

D-A-T			0.6		0.8		1.0
D-A	0.1	0.5	0.6		0.8	0.9	1.0
D-T			0.6	0.7	0.8		1.0
I							

Table 5A Amplitude peaks that exceed LS after the subsynchronous region in pump mode.

D-A-T	D-A	D-T	I
		1	
		1	
		1.6	
2	2	2	
		2.4	
			2.5
	2.7		
3	3	3	
3.4	3.4	3.4	
		4	
			4
			4.2
4.9	4.9	4.9	
		5	
5	5.4	5	
6	6	6	
	7.8		
			8.3
	9.3		
	9.8		
	12		
	14.7		
	19.7		
			20.8
	21.6		
	23.6		
	23.7		
	23.9		
	24.6		
	24.7		

Table 7A Amplitude peaks that exceed LS after the subsynchronous region in turbine mode.

D-A-T	D-A	D-T	I
	1.1		
1.2	1.2	1.2	
	1.3		
	1.4		
		1.6	
2	2	2	
		2.1	
		2.2	
		2.5	
		2.6	
		2.7	
2.8	2.8	2.8	
2.9	2.9	2.9	
3	3	3	
		3.1	
		3.2	
3.3	3.3	3.3	
		3.4	
		3.5	
		3.6	
		3.7	
		3.8	
		3.9	
4	4	4	
		4.1	4.1
		4.2	4.2
		4.6	
4.9	4.9	4.9	
5	5	5	
5.4	5.4	5.4	
	5.9		
6	6	6	
	6.2		
	7.8		
	8.2		8.2
	8.8		
	9.3		
	9.8		
	12		
	13.7		
			20.6
	21.6		

Table 6A Amplitude peaks exceeding LS in the subsynchronous region in turbine mode.

D-A-T	D-A	D-T	I
		0.1	
		0.2	0.2
0.3	0.3	0.3	
0.4	0.4	0.4	
0.5	0.5	0.5	
0.6	0.6	0.6	
0.7	0.7	0.7	
0.8	0.8	0.8	
	0.9		
1	1	1	

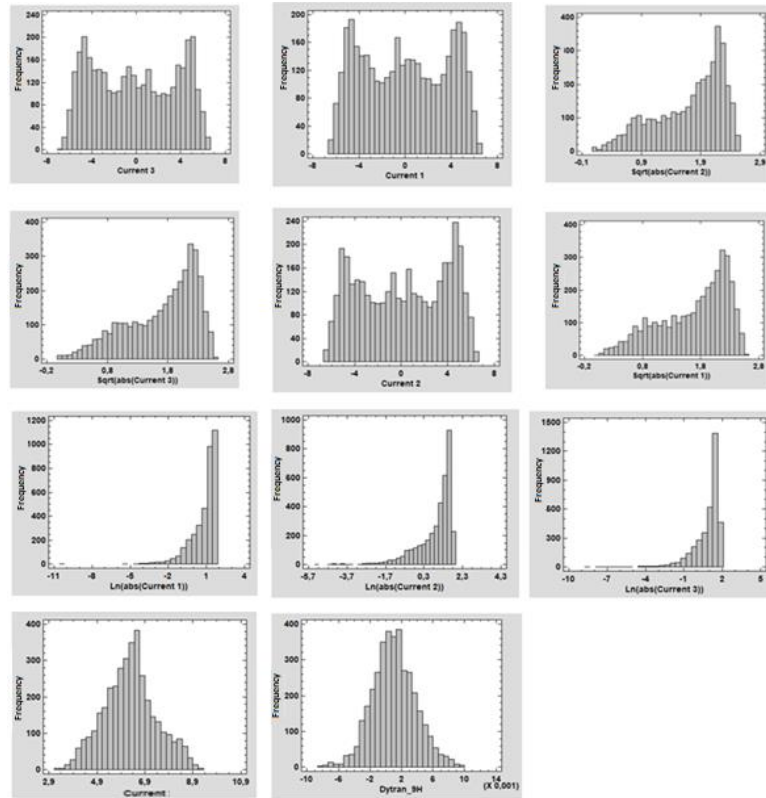


Fig. 1A. Histograms for the variables under study in pump mode.

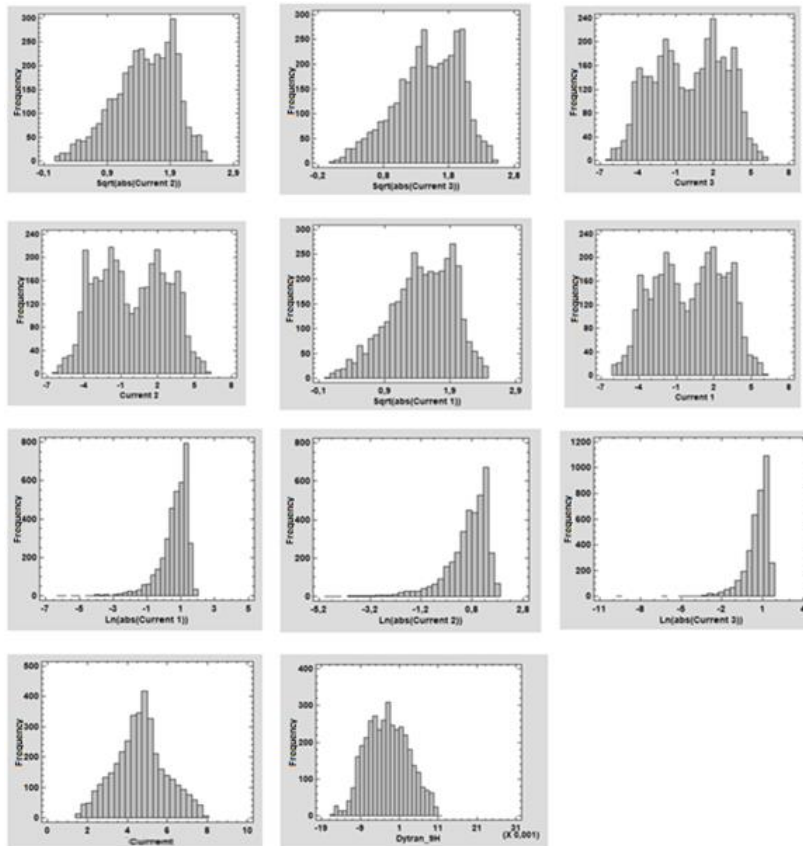


Fig. 2A. Histograms for the variables under study in turbine mode.

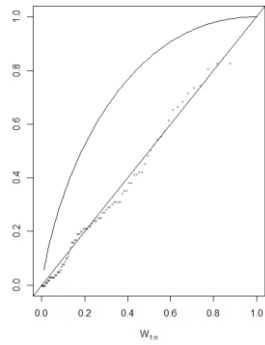


Fig. 3A. Chi-plot graph for copula adjustment in pump mode.

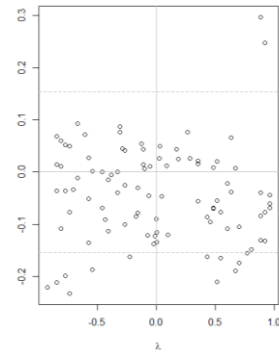


Fig. 4A. K-plot graph for the copula fit in pump mode.

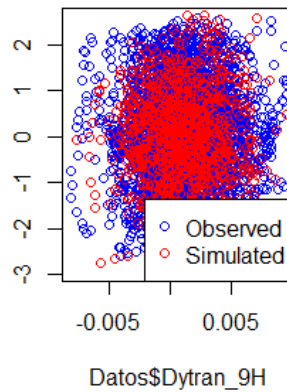


Fig. 5A. Comparison of fit with observations

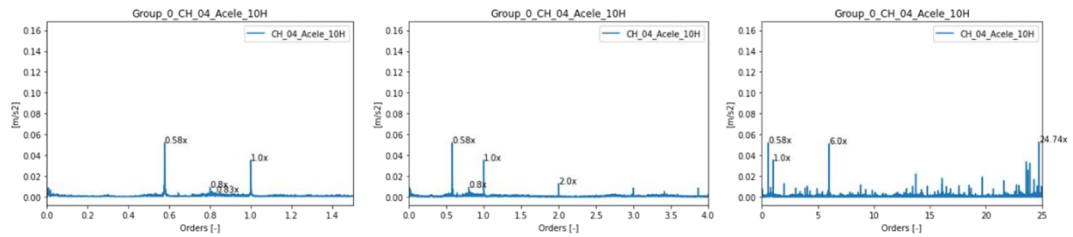


Fig. 6A. Spectra for the accelerometer variable in pump mode

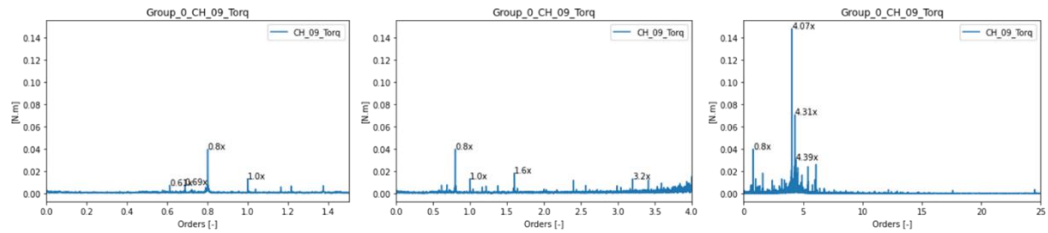


Fig. 7A. Spectra for the Torque variable in pump mode

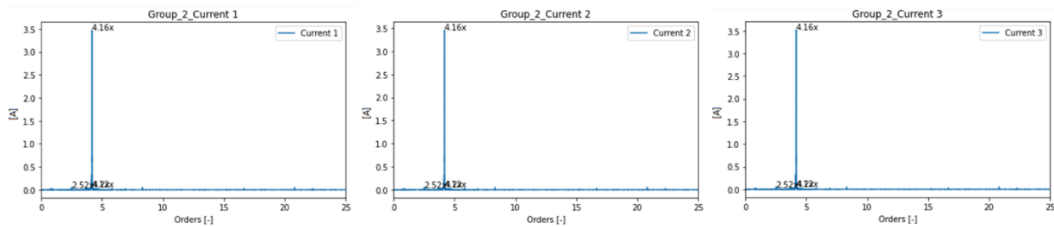


Fig. 8A. Spectra for currents in pump mode.

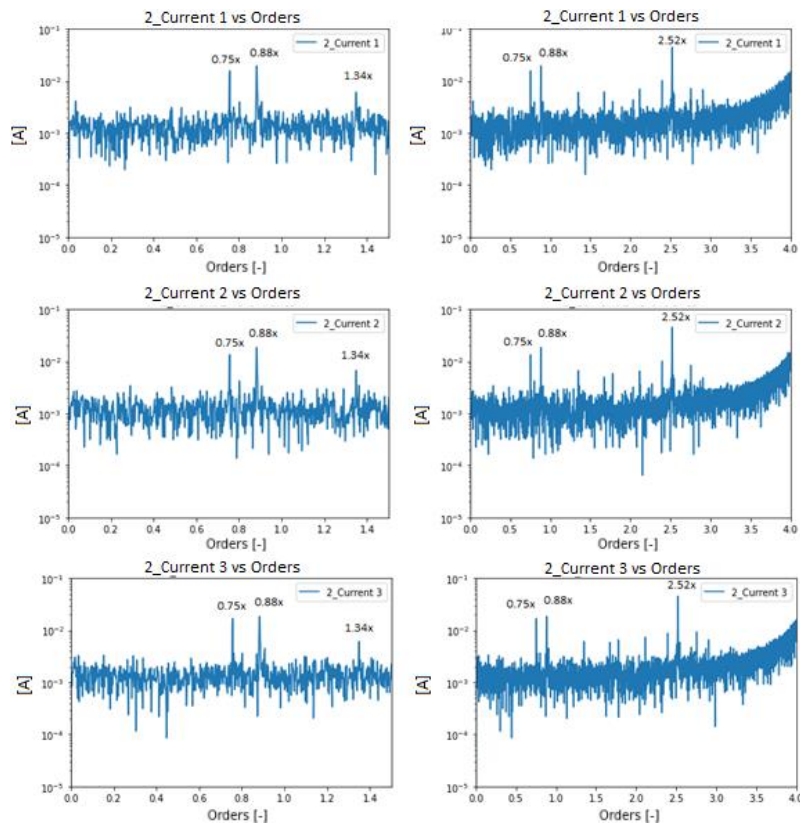


Fig. 9A. Spectra of the currents in logarithmic scale for the pump mode.

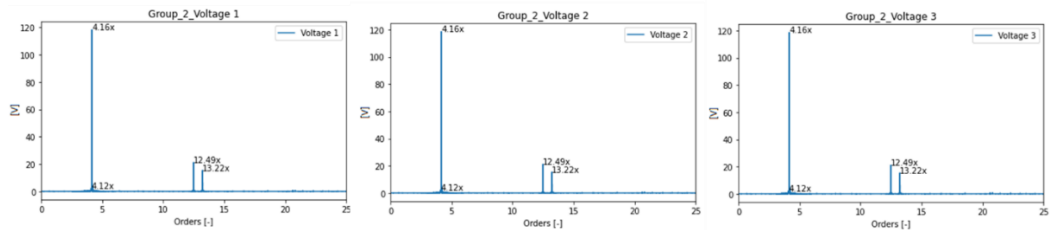


Fig. 10A. Spectra for the voltages in pump mode.

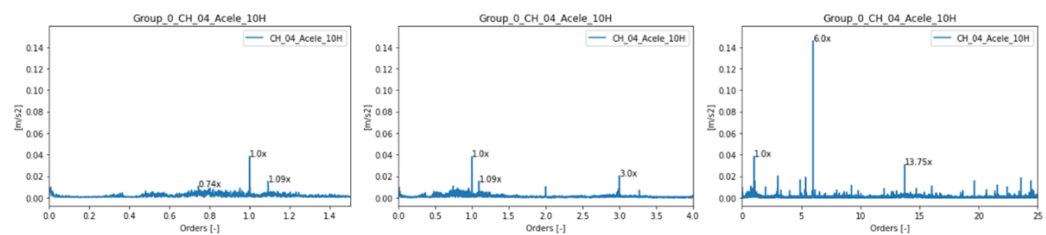


Fig. 11A. Spectra for the variable accelerometer in turbine mode.

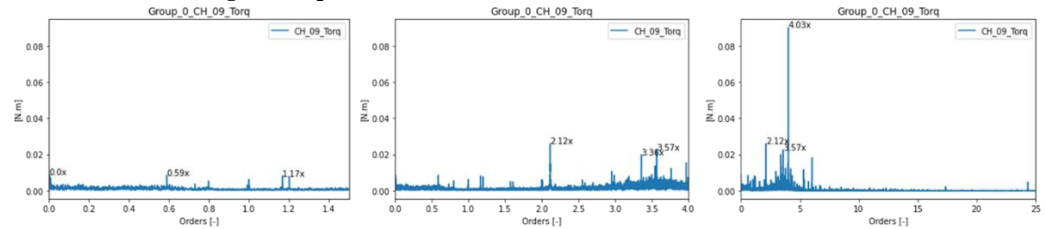


Fig. 12A. Spectra for the torque variable in turbine mode.

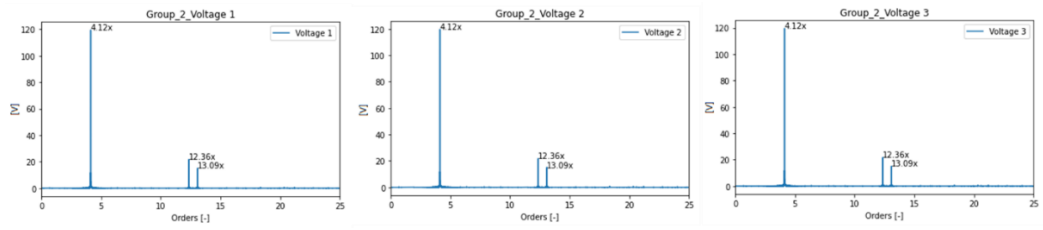


Fig. 13A. Spectra voltages for the turbine mode